

Manufacturing Letters

Manufacturing Letters 41 (2024) 113-123



52nd SME North American Manufacturing Research Conference (NAMRC 52, 2024)

3D Soft Material Printer as a Mesoscale Additive Biomanufacturing Platform for In-Space Manufacturing

Albert J. Patrick, Salil Bapat, and Ajay P. Malshe*

Manufacturing and Materials Research Laboratories (MMRL), School of Mechanical Engineering, Purdue University, West Lafayette, IN 47907, United States

* Corresponding author: E-mail address: amalshe@purdue.edu

Abstract

With the burgeoning in-space manufacturing (ISM) industry, developing an on-demand additive manufacturing (AM) platform will be crucial for long-term space habitation. However, acute space boundary conditions, such as limited physical space, microgravity, vacuum, and others pose unique challenges for designing the printing process, the platform's structure, and the materials' printability. An AM platform operable in a space environment would enable production at the point of need (PoN), for example, on-demand food, nutrition, and pharmaceutical products. This research is focused on the design, fabrication, and testing of a 3D printer confined within CubeSat boundaries to study the feasibility of soft material printing aimed toward potential ISM applications. The printer unit was built using components off the shelf (COTS) while adhering to the severe spatial boundary conditions posed by the CubeSat dimensions and was tested using an edible material ink to demonstrate multi-layer prints of soft materials. Printing in ambient Earth conditions as well as under vacuum displayed consistent layer cohesion and comparison to 3D model data although vacuum prints showed visibly dehydrated prints owing to outgassing of air bubbles. The printer equipment's structural integrity was validated under simulated launch and operation conditions using a vibration testing setup according to the NASA-recommended microsatellites standards. The results indicated that the printer assembly maintained its structural and operational integrity during and after testing. Using soft materials as the basis of testing allows scalability when expanding to more complex and structural materials to produce spare parts using a frugally engineered modular manufacturing platform.

© 2024 The Authors. Published by ELSEVIER Ltd. This is an open access article under the CC BY-NC-ND license (https://creativecommons.org/licenses/by-nc-nd/4.0)

Peer-review under the responsibility of the scientific committee of the NAMRI/SME.

Keywords: In-space manufacturing (ISM); 3D printing; additive manufacturing

1. Introduction

In-space manufacturing (ISM) is a method for producing parts for assembly and services, for Earth and space, not capable of being manufactured on Earth or providing an additional benefit due to processing under microgravity. ISM research has gained significant attention over the years with demonstrations on the International Space Station (ISS) for various products of interest fabricated under microgravity conditions. Although expensive launch costs and a non-existent supply chain mean that achieving scalability and progressing

from 'making' to 'manufacturing' remains challenging. This challenge is further compounded by the extreme boundary conditions of habituating in space such as limited physical space, lack of an atmosphere, and cosmic radiation. Design and development of modular manufacturing equipment could alleviate some of these challenges by providing versatility and multifunctionality which is the focus of this paper. To address the limited physical space constraint, this research aims to demonstrate the use of a CubeSat system as a mesoscale AM platform for usage in the space environment and a demonstration testbed platform. The experimental focus is on

1) designing a 3D printer equipment that conforms to stringent spatial boundary conditions posed by the CubeSat, 2) manufacturing and assembly of the printer equipment, 3) verifying the integrity of the printer design under simulated space launch and vacuum conditions, and 4) to study the feasibility of extruding soft material using chocolate for demonstration per the ASTM definition of 3D printing.

Nomenclature

ISM In-space manufacturing

ISAM In-space servicing, assembly, and manufacturing

AM Additive Manufacturing 3DFP 3D Food Printing

COTS Components off the shelf

PoN Point of Need

1.1. Literature Review of In-Space Manufacturing

ISM is an emerging field of innovation within manufacturing extending the envelope of manufacturing processes beyond the traditional terrestrial usage to operate under extreme boundary conditions and environments of space. The authors define ISM as a form(s) and/or methodology developed using in situ space boundary conditions for travel and/or to reside and/or grow sustainably at or above the Kármán Line. The Kármán Line is 100 kilometers (about 62.14 miles) above the surface of the Earth, where one begins to experience the effects of reduced gravity. The moon is the closest celestial body to travel to and is a great candidate to support a future human outpost to refuel food and other resources. However, the lack of atmosphere unpredictability of the environment make it less desirable as a long-term human outpost rather than just a refueling station. For example, the temperature variation (111 °C to -171 °C) at the Apollo landing sites poses significant thermal fatigue challenges to surface structures due to the thermal expansion/contraction [1]. Hence, ISM efforts addressed through on-orbit manufacturing either on the international space station or the commercial space stations in the future offer merit and research consideration.

The advantages of ISM make it attractive in commercializing space travel and habitation. Cost and time constraints restrict quick responses to damaged parts due to unfeasible resupply missions [2]. ISM could provide rapid and on-demand solutions for part failure repairs while enabling cheaper, faster, and more sustainable systems in the new space economy [3].

Challenges of ISM are dependent on the location of the manufacturing process occurring. Current in-space servicing, assembly, and manufacturing (ISAM) road mapping conferences have discussed and determined the difficulty associated with overcoming the challenges of ISM [4] Intravehicular ISM incurs unique challenges that extravehicular ISM doesn't encounter and vice versa. The main challenges include microgravity effects, process safety, and platform constraints (e.g., limited footprint, and power) [5]. External space environment challenges (low vacuum pressure, extreme temperature variation, space debris and junk, radiation, etc.) pose an immediate challenge to manufacturing [4–6]. Development of a microsatellite with low physical footprint could be beneficial for ongoing space infrastructure

due to being available and accessible. Design and construction of space infrastructure requires capability of accommodating diverse environments and conditions while enabling distributed points-of-need (PoN) operations [3,7]. CubeSats or miniaturized satellites present a relatively low-cost, high-value test vehicle for conducting scientific experiments and have progressed from being educational tools to offering an opportunity for fundamental science and engineering research From a manufacturing perspective, additive [8]. biomanufacturing processes are of specific interest and are well-known for allowing the democratization of manufacturing on Earth by enabling mass-scale customization and for ondemand, on-site operation to manufacture one-of-a-kind parts. The following subsection provides a brief overview of AM approaches in the context of ISM.

1.2. Literature Review of 3D Printing for Biomanufacturing

The ASTM definition for additive manufacturing (AM) is "the process of joining materials to make objects from 3D model data, usually layer upon layer, as opposed to subtractive manufacturing technologies" [9]. AM has several different processes for producing 3D objects. The main methods include fused deposition modeling (FDM), AM of powders by selective laser sintering (SLS), selective laser melting (SLM) or liquid binding in three-dimensional printing (3DP), as well as inkjet printing, contour crafting, stereolithography, direct energy deposition (DED) and laminated object manufacturing (LOM) [4,10]. Due to the restrictions of space boundary conditions, techniques not utilizing gravity in their layer-by-layer process are used in a space environment. Powder-based and dropletbased methods have been tested in low gravity via drop towers or parabolic flights but have not been tested in space. Fused filament fabrication (FFF) has been used in space aboard the International Space Station (ISS) to demonstrate the fabrication of a ratchet wrench using acrylonitrile butadiene (ABS) [4]. Currently, FFF can process thermoplastics such as acrylonitrile, polylactic acid, high density poly ethylene, and polycarbonate but can also indirectly process ceramics and metals [4,11–13]. With further research into AM processes in low gravity, the advantages of AM would become more prevalent for long-term space habitation. This paper focuses on the development of an extrusion-based additive manufacturing platform for potential ISM applications for soft materials using soft edible materials for demonstration case study.

Highly customizable and personalized food using 3D food printing (3DFP) is the latest technique in additive manufacturing [14]. Soft material extrusion has been around using pipets for frostings, custard, cheeses, etc. Mechanical and rheological properties of soft materials such as food determine their printability. Rheology refers to studying a food system's flow under controlled conditions in which multiple components, including viscosity, shear stress, shear rate, loss modulus, storage modulus, and yield stress, are considered [15]. Food products behave similarly to polymers having elastic and viscous properties that can change depending on external factors. For successful printing, the material must flow through the nozzle in the extrusion process. Printability is defined as the successful printing of a material by the selected printer equipment while maintaining the structural integrity and shape of the printed object [15]. Critical factors for controlling printability are material properties of food formula or food inks, and the optimization of printing variables [16]. Depending on the material used, nutrients can be manipulated and tailored to cater to the user's needs. The customization could reach beyond existing nutritional preferences to converge with personalized nutrition, in which a diet is personalized to an individual's health status and body type requirement [17]. For space missions, 3D printing would allow for relatively simple food-making in space and longer shelf life storing cartridges [18,19].

Currently, NASA uses freeze-dried material to feed astronauts. Due to the low drying rate, there is high energy consumption, low production yield, and high operating cost [20] associated with this operation. The freeze-drying technique retains nutritional ingredients allowing a high level of quality for aerospace food with a long shelf-life of three to five years [20]. Freeze-dried food has advantages; however, the food must be resupplied from Earth. Depending on the material used, 3D-printed food can be complemented with freeze-drying to extend the shelf-life. The results of 3D-printed semi-solid objects post-processed by freeze-drying were a porous, lowdensity, and crunchy matrix that prevented shape deformation and extended the shelf life [21]. With the ability to customize various characteristics of food products, i.e., shape, texture, color, flavor, and nutrition, 3D printing can be extended past the application of structural manufacturing to the culinary sector [22]. With improved mechanical properties, the 3Dprinted food would maintain shape and form, adding to the aesthetics of the printed food. 3D printing of food products can be customized to the person to address flavor and nutritional demands [23]. Nutrition is more than just food; it can also be the production of medicine and health-related products. Food science research overlaps with the nutritional health of space explorers affecting many other aspects of space medicine and physiology including psychological health, sleep and circadian rhythmicity, taste and odor sensitivities, radiation exposure, body fluid shifts, and wound healing and changes in the musculoskeletal, neurosensory, gastrointestinal, hematologic, and immunologic systems [23].

Using the CubeSat vehicle platform to perform 3D printing operation poses stringent boundary conditions on the equipment design, however it 1) showcases the ability to print mesoscale geometries that can later be utilized for more advanced additive manufacturing, 2) uses less physical space to produce products as a part of frugal engineering methodology, and 3) proves that biomanufacturing can be performed in a space environment. CubeSat systems traditionally have not been used for AM but have flown biological missions, making them good candidates for this case study. Biomanufacturing for space can be expanded past food products and can assist in tissue engineering and pharmaceutical development. This paper explores using soft materials (food products, as a case study) for use in simulated space environment conditions including a restrictive workspace of a CubeSat as an equipment demonstration case study. The intended focus is more on development of the equipment to demonstrate 3D printing in space environment and not on the materials and manufacturing research pertaining to additive manufacturing (e.g., impact of process and material variables on printing, print quality optimization etc.). The sections below discuss the design and fabrication of mesoscale 3D printer followed by the experimental results of soft material printing. In line with the intended motivation of this work, the structural integrity of the printer equipment is experimentally validated under simulated launch conditions (vibration testing and vacuum testing) along with printability under vacuum environment.

2. Development of Design of 3D Soft Material Bioprinter

The severe physical space constraints of the CubeSat system and space boundary conditions dictated the design of the 3D soft material printer. The CubeSat system restricted the physical size and weight of the printer and power consumption. Additionally, once launched within the CubeSat module, the printer must operate remotely thus requiring a programmable operation via online control. Space boundary conditions include low gravity and vacuum pressure and extreme temperature variation. Table 1 lists the internal (CubeSat constraints) and external (in-space constraints) affecting the printer. It must be noted that the external skins of commercial CubeSat modules typically include provisions for energy harvesting and EMI shielding and thus are not discussed below. The researchers view CubeSat as a commercial component off the shelf that can be utilized as a test vehicle platform by housing the printer module internally.

Table 1. Internal and External Boundary Conditions affecting the printer

	nai Boundary Conditions affecting the printer
Boundary Condition	Description
Physical Space	The CubeSat system for a one cube unit's outer
	dimensions is $10x10x11$ cm. The 3-cube unit is
	used and the exterior dimensions are 10x10x34
	cm. However, within the CubeSat, to account for
	shielding, the maximum values of the printer can
	be 9.3x9.3x22.7 cm ³ .
Power Consumption	The amount of power the printer can consume
	cannot exceed 17 watts.
Weight	The weight of the printer cannot exceed 6 kg.
Operation Source	The printer must be able to operate remotely due
	to the expectation of being launched into space
	with no further human interaction after launch.
Low Gravity	The force of gravity in low Earth orbit is
•	approximately nine m/s ² , only slightly less than
	the gravity on Earth.
Vacuum Pressure	The pressure in low Earth orbit ranges from 10 ⁻⁶
	to 10 ⁴ Pascals. Reduced pressure influences
	materials with higher air content in them.
Launch Vibration	NASA STD 7001B Payload Vibroacoustic Test
	Criteria recommend minimum component
	vibration workmanship test to identify any latent
	flaws within the system at an electromechanical,
	electrical, and electronic level [24].
Material	The printer must be made of a space-rated
	material. Currently, it is designed with
	Polylactic Acid (PLA) and is expected to be
	expanded to anodized aluminum for the entire
	system.
Temperature Extremes	The temperature ranges from -65°C to 125°C. In
F	dark spots, the temperature will reach below-
	freezing temperatures, which requires the
	system to be well-insulated to counteract the
	temperature. Extreme temperatures can affect
	soft material printability and electrical systems.
	son material printaginty and electrical systems.

Fig. 1(a) shows the final design of the printer that was used for testing. The printer design went through several design iterations (not discussed here) spanning various mechanisms for material delivery and consolidation as well as various translational modes for the printer nozzle. The design iteration also included changing the placements of drive motors, Z-axis movement, and the physical positioning of the printing nozzle

and substrate. Some of the iterations of the printer consisted of various choices that were unsuited for completing the ASTM definition of additive manufacturing and thus were modified. These iterations were targeted towards improving the functionality and manufacturability of the printer module.

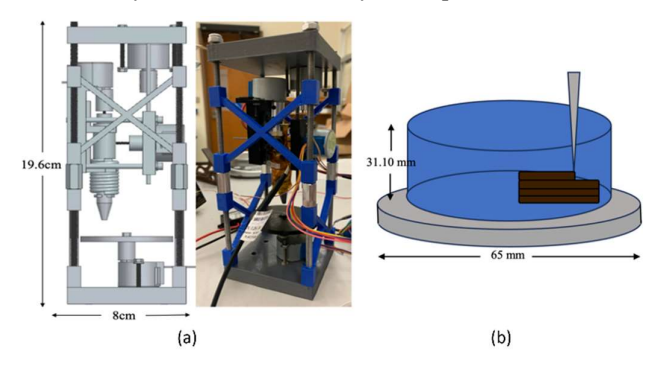


Fig. 1. (a) Final design and assembly of the 3D Mesoscale Bioprinter (b)

Build volume of the printer

The dimensions of the final design were approximately 8x8x19.6 cm³ (compared with 10x10x34 cm³ dimensions of a 3-cube unit CubeSat). The Z clearance of over 10 cm was necessary to allow for the installation of the auxiliary performance modules such as power modules, controllers, and other wiring. The maximum allowable printing build height is 31.10 mm (about 1.22 in) based on the syringe extruder motor contacting the bottom face of the top plate of the printer. As depicted in Fig. 1b, the build volume of the printer is approximately 25.01 cm³. The extruder syringe is made of aluminum and holds 1,778.96 mm³ of material with the piston in place. The syringe nozzle has a diameter of 2.3 mm (about 0.09 in) and is spring-loaded to stop material from escaping. The most common manufacturing process used in 3DFP research is material extrusion due to the variety of food materials, like chocolate, being capable of extrusion [25]. The printer was designed to extrude viscous materials to deposit layers. The material was melted in the middle of the syringe and deposited onto the printing bed. The print jobs were achieved by rotating the printing stage and activating the radial motor and z-axis motor. The plate would be rotated to create designs using polar coordinates. The heating element used was an induction heater to melt the material close to its melting point to allow extrusion. The heat was transferred to the syringe via conduction. The design also utilized the introduction of truss structures (blue PLA crossbeams seen in Fig. 1) on the sides to provide extra stability during vibration testing.

The printer can be programmed for remote operation by utilizing an Arduino MEGA 2598 microcontroller to control printing. There was an initial delay (dwell time) before the start of each print to allow for sufficient heat to build for extrusion. The code was uploaded beforehand and when connected to an external power bank the printer would begin the sequence. This allowed for remote operation via user control as the printer would not activate until power was attached and ran the uploaded code until completion without further user input. The initial delay was 30 to 45 seconds to allow any external processes to be completed, i.e., reaching the vacuum pressure necessary during vacuum printing testing. The following

section provides a detailed description of the experiments and characterization methods.

3. Experimental details

This section outlines the preparation protocol for the food ink preparation, printing methodology under two distinct pressure conditions (ambient and vacuum) as well as the details for vibration testing. The purpose of printing experiment was to test the printing functionality of the printer while the vibration testing was performed to study the robustness of the printer equipment in response to the launch conditions.

3.1. Preparation of chocolate-based material ink for 3D Printing

The popularity of using chocolate in 3DFP comes from its melt extrusion capabilities and use in the high-end food industry [26]. To prepare the chocolate ink for printing, chocolate Chips (brand: Great Value) and heavy whipping cream, at a ratio of 3:1, were melted in a small pot at low heat (29°C) with continuous stirring until smooth consistency was achieved. This ratio was determined from the initial trial experiments to achieve the right consistency and flow properties. It was then extracted using a 100 mL syringe and filled to around 40 mL. The syringe was chilled to allow the chocolate to become firm again before depositing it into the extruder nozzle.

3.2. Methodology for varied pressure testing

For ambient pressure testing, the environment was kept at approximately room temperature (19-21°C) and the pressure was 1.128 atm. The optimal printing temperature was 27°C approximately five degrees less than the chocolate melting temperature. The design to be printed was uploaded to the microcontroller. A larger (100 mL) syringe was used to supply chocolate into the extruder by manually filling the extruder under ambient pressure conditions. The maximum volume of the extruder syringe was approximately 1,778.96 mm³ or 1.78 mL. The piston for the extruder syringe was set to engage slightly with the extruder medium to allow proper translation when activated. The initial delay for the printer was 45 seconds.

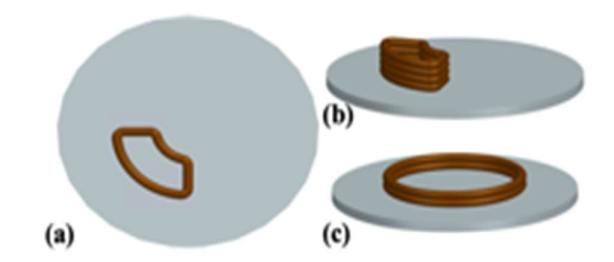


Fig. 2. (a) Top view of the quarter circle design (r_o=18.70, r_i=12.90), (b) isometric view of the quarter circle design, (c) isometric view of the full circle design (φ21.50).

Once the printing sequence is activated, the motor extrudes material for the quarter circle design (Fig. 2a and Fig. 2b). The printing bed is rotated counterclockwise in incremental steps three times, depositing chocolate per step to print the inner diameter. The radial motor then activates to change the radius of the printer head. Once in position, the printing bed rotates

clockwise in incremental steps one-twenty-fourth of a full circle to print the outer layer. The small incremental extrusions are to account for the change in radius to not break the chocolate in between extrusions. This returns the extruder syringe to its original position. Once the first layer is completed, the extruder syringe is translated into the z-axis for 3.6 mm, and the process is repeated until the extruder syringe is empty.

To print the full-circle design (Fig. 2c), the extruder was activated and then rotated in twelve incremental steps in a circle, extruding chocolate per step until completing one layer. Once in the original position, the z-axis motor translates 3.6 mm upward in the z-direction to begin the next layer. Success was determined by the structural integrity of the print, visual layer adhesion, and resemblance to the input design. Printing parameters for the test are shown in Table 2. To print the same design under vacuum pressure, similar printing parameters were utilized with the addition of the initial and final printing pressure. Temperature was recorded throughout the test as the induction heater was not utilized.

Table 2. Parameters for ambient pressure printing

Design	Full Circle with Air Vents	
Nozzle Diameter (mm)	2.30	
Initial Nozzle Height (mm)	4.61	
Volumetric Flow Rate (mm ³ /s)	4.88	
Shear Rate (s ⁻¹)	5.40	
Printing Temperature (°C)	27.22	

The testing also studied the effect of vacuum conditions, e.g., on printing medium and printed samples when placed in an unpressurized vessel. Table 3 represents the parameters used during the vacuum chamber printing. At the start of the test, the environment was kept at approximately room temperature (19-21°C) and the pressure was 1.128 atm. The vacuum chamber pressure was gradually decreased until it reached quasiequilibrium, then the printer was activated. This ensured the material would survive the low-pressure system before printing. The full circle design was printed due to the simplicity of the design and for performing comparisons between ambient pressure and vacuum pressure prints. As compared to the ambient printing experiment discussed above which used 1.78 mL of material ink, the amount filled into the extruder syringe for vacuum pressure printing was reduced to 1.3 mL to allow for the expansion of the medium during the outgassing procedure.

Table 3. Parameters for vacuum chamber printing

Design	Full Circle with Air Vents
Nozzle Diameter (mm)	2.30
Initial Nozzle Height (mm)	4.61
Volumetric Flow Rate (mm ³ /s)	4.88
Shear Rate (s ⁻¹)	5.40
Initial Temperature (°C)	23
Final Temperature (°C)	21.67
Initial Printing Pressure (mTorr)	450-500
Final Printing Pressure (mTorr)	350-400

For printing under vacuum conditions, the chocolate-based material ink was loaded into the syringe and placed into the vacuum chamber to remove air bubbles within the syringe and the medium. Air vents were necessary to allow for the air bubbles within the chocolate medium to be released when the piston was applied during the second vacuum treatment. After two vacuum treatments, the piston for the extruder syringe was set to slightly engage the extruder syringe to provide proper translation when activated. The initial delay time was also extended to two minutes to allow the vacuum chamber's pressure to decrease and stabilize before printing started.

3.3. Vibration testing and hammer impact testing methodology

The random vibration testing on the printer was conducted to simulate the launch conditions the CubeSat will experience when mounted in the launch vehicle. The random vibration test is designed to be non-deterministic and vibrates at all frequencies across a specified range. The parameters and procedure for the random vibration testing are as follows: (1) vibration was set at 20 Hz at 0.01 g²/Hz; (2) gradually increasing from 20 Hz to 80 Hz at +3 dB/oct; (3) remaining constant from 80 Hz to 500 Hz at 0.04 g²/Hz; (4) then gradually increase from 500 Hz to 2,000 Hz at -3 dB/oct, and (5) finally vibrated at 2,000 Hz at 0.01 g²/Hz. Each frequency was maintained for three minutes. The printer was bolted to the DB-139 DuoBase shaker. The above-described minimum component workmanship test for small payloads weighing less than 50 kg is cited in the Launch Space Program: Program Level Dispenser (LSP-REQ-317.01 Revision B) and NASA Standard 7001B Payload Vibroacoustic Test Criteria. The test performed to identify manufacturing and any component/structural flaws. This test was performed three times along each direction (x, y, and z axes). The test was considered successful if there were no parts/components malfunctioning and/or getting damaged after vibration testing and the top plate's displacement was within the limits set by the CubeSat requirements. The amount of displacement was recorded in the x and y-axes but the amount in the z-axis was negligible. To record the data, each corner of the top plate was measured from the top of the top plate to the bottom of the bottom plate. After the vibration test was run the corners would be remeasured to record the amount of displacement that occurred.

A hammer impact test was conducted to determine the resonant frequency and coherence of the printer. The resonant frequency is the natural frequency of vibration determined by the vibrating object's physical parameters, and coherence is the measure of two signals at the same frequency. The coherence graph verifies that a peak observed in a transfer function, i.e., resonance frequency test, is a resonant frequency of the device under testing. The printer was bolted down to the shaker for stability and a fixed point to perform the test. Accelerometers were placed around the printer on the top plate, syringe apparatus, and radial motor. Each accelerometer corresponds to its position on the printer. Accelerometer 1 (accel. 1) was placed on the top of the printer, Accelerometer 2 (accel. 2) was placed on the back of the syringe apparatus, and Accelerometer 3 (accel. 3) was placed on the back of the radial translation motor. From there the printer was tapped in the x, y, and z directions to analyze the amount of vibration that traveled through the printer when struck by the hammer. The hammer

and accelerometers recorded the data and sent it to the program to be analyzed and recorded. When the printer is struck, the transfer function (g/N) is recorded as a function of frequency. The recorded coherence verifies the resonant frequency to determine if the vibration force applied and the system's reaction are linear.

4. Results and Discussion

Results of printing and characterization under different pressures (ambient and vacuum) and vibration testing are discussed below in the visual demonstration of prints, viscosity studies, random vibration testing, and hammer impact testing.

4.1. Printing results

4.1.1. Full circle design under ambient and vacuum conditions (Varied pressure printing)

The full-circle design prints were used to compare the printing process under ambient and vacuum chamber conditions. The quarter circle design was performed to demonstrate movement along all three axes and to prove multilayer building in a three-dimensional design geometry. The designs were each printed three times and the averaged values are reported below. The design of the extruder syringes changed the amount of chocolate inserted into the extruder syringe. The 'full circle' design used the extruder syringe before the addition of air vents, which were necessary for the vacuum chamber printing tests. Results of the ambient Earth pressure printing are displayed in Table 4 and Table 5. The printing process was repeated with the same print conditions and process parameters to prove reproducibility and demonstrate the 3D printability of the proof-of-concept design. Apart from a minor test to test variations in the measurements due to slight changes in the starting points, overall, the repeat experiments showed a consistent trend. The initial nozzle height's position was kept consistent because it correlated with chocolate connectivity and continuity during extrusion. If the nozzle height is too high, then the chocolate gets extruded in a discontinuous fashion which is deemed undesirable. The percentage difference from the CAD design is the most important as it accurately displays the printer's limitations in terms of precise placement and resolution. In the full circle design, the percent difference in the diameter from the CAD design is 29.7%. In the quarter circle design, the percent difference in the radius (inner and outer) from the CAD design is approximately 26.8%. Fig. 3a and Fig. 3c display the final result of the ambient Earth pressure printing process in an overhead and side view. Two layers are printed to allow for comparison with the vacuum pressure printing process where the amount of chocolate filled in the extrusion syringe was limited (equivalent to two layers of printing) due to outgassing issues.

Vacuum chamber environment printing maintained the same parameters as ambient pressure printing. During outgassing cycles, air bubbles are removed from the chocolate. The printing process produces a print with a dehydrated appearance and micro-pores on the surface (Fig. 3b and 3d). The low ambient pressure caused the additional heat from the induction heater to cause the dehydration of the chocolate and thus viscosity to decrease resulting in prints where the design could not retain structural integrity.



Fig. 3. (a) Overhead view of the complete circle design printed in ambient pressure; (b) overhead view of the complete circle design printed in vacuum chamber pressure; (c) side view of complete circle design in ambient pressure displaying distinct printed layers; (d) side view of complete circle design in the vacuum chamber pressure displaying distinct printed layers.

Ultimately, the heater was not used for the vacuum chamber prints because the reduced pressure lowered the melting point. The additional heat would lower the viscosity to the point where structural integrity was sacrificed. The addition of the air vents on the extruder syringe caused a reduction in the total printing material used because when outgassing occurred the material would rise and extrude prematurely from the top of the syringe. The discontinuity in the print pattern could be attributed to the lack of liquid content due to the outgassing and resulting dehydration reducing the consistency of the material.

Table 4. Results of the Full Circle Design

Design	CAD Design	Full Circle with Air Vents
Average Diameter (mm)	21.50	27.88
Single Layer Print Height (mm)	2.30	2.30
Final Print Height (mm)	4.6	5.16
Printing Time (s)	N/A	360

Table 5. Results of the Quarter Circle Design

Design	CAD Design	Quarter Circle
Inner Radius (mm)	12.90	16.32
Outer Radius (mm)	18.70	23.66
Single Layer Height (mm)	2.30	2.30
Final Height (mm)	9.2	8.64
Printing Time (s)	N/A	617

4.1.2. Demonstration of printing quarter circle test structures

Printing the quarter circle design was done to display the full capabilities of the printer. The printing bed's limited physical space does restrict the prints' size of the prints but translation in three dimensions fulfills the ASTM definition for AM. The printed design also displays more than two layers with interfacial connectivity. Fig. 4 displays the quarter-circle design with four layers of chocolate extruded before the syringe is empty. The layer-to-layer adhesion is clearly visible and thus

is considered a successful demonstration of multi-layer print. Future advancements could include optimization of the extrusion material ink to control the flowability and spread to enable more precision placement of the deposited material.





Fig.4. Quarter Circle design displaying four layers of chocolate.

4.1.3. Viscosity study of standard and vacuum-chocolate

To determine if there is a significant difference between the viscosity of the chocolate when printed in ambient pressure and reduced pressure, the viscosity of the chocolate was measured using the TA Instruments Discovery RH-3 rheometer. The test was conducted by stabilizing the temperature and performing a logarithmic sweep of the shear rate to determine the viscosity. The temperature was varied by 3°C ranging from 21°C to 33°C. Due to the operating temperature of the printer being 27°C, the range of testing was at melting temperature (30°C to 33°C) and at lower temperatures to display higher initial viscosities. Fig. 5 displays the viscosity decreasing as the shear rate increases and displays shear thinning properties. Noticeably at 27°C and 30°C the chocolate had lower initial viscosities, which would make them the optimal temperature for printing. All temperature variations eventually averaged less than 50 Pa·s at the operating shear rate of 5.4 s⁻¹.

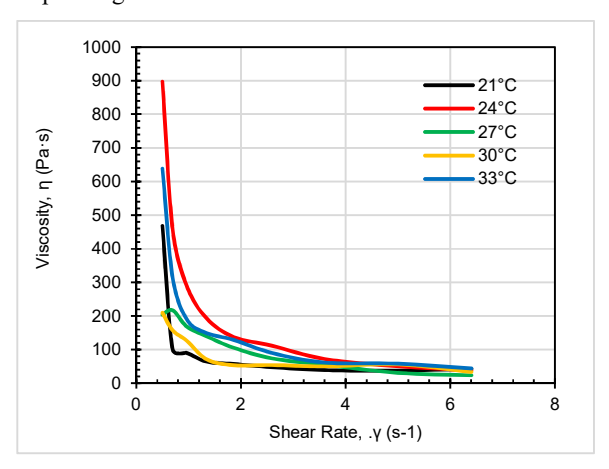


Fig. 5. Standard chocolate tested at constant temperature across various shear

To compare standard (S) ambient condition chocolate and vacuum-cycled (VC) chocolate, the same test was conducted to determine if the viscosity was higher for vacuum-cycled chocolate. The results showed higher viscosities at the operating shear rate than the standard chocolate. Fig. 6 displays the data acquired from the viscosity of standard chocolate versus vacuum-cycled chocolate as the shear rate increases and the temperature is constant.

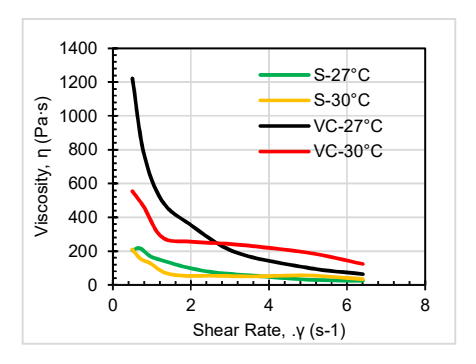


Fig. 6. Viscosity of standard and vacuum cycled chocolate tested at constant temperature across various shear rates

4.1.4. Printer accuracy

There was a noticeable difference between the CAD file and actual print in comparison to other 3D printers commonly used on Earth. This printer inaccuracy is likely due to the equipment components being slightly different than the CAD file data, printer set-up differences, and the printing process being executed one line of code at a time. Another inaccuracy in the print is the "waviness" of the layers. The printing bed is made using 3D-printed parts and is locked into place using a keyhole. When the plate is locked into place the printing bed tilts due to pressure being applied from the tightness of the slot for the printing bed. The other reason for the waviness could be the use of a less sophisticated microcontroller. The printer would be able to make designs more closely resembling the CAD model by addressing some of the above limitations in the future.

Printing under different pressures (ambient vs vacuum) resulted in visually different prints. Along with visually different prints, the initial viscosity of vacuum-cycled chocolate was higher, and the viscosity was still higher once reaching the shear rate of the printer. The higher viscosity could also affect the printing accuracy because the printer settings were not changed between the ambient pressure and vacuum-cycled prints. For future tests, the shear rate would have to be adjusted to allow for the same viscosity as when printing standard chocolate.

Varying the pressure while maintaining the design required a different methodology for printer loading. Ambient pressure doesn't require a vacuum treatment and utilizes the induction heater to produce the required viscosity. The decrease in pressure directly affected the use of a heating element due to the heat accumulation of the motors during usage. If the heat accumulated by the motors is not distributed correctly, the heat could damage the motors and subsequently damage the printer and lead to malfunctioning during operation. In space, heat must be removed through conduction; within the vacuum chamber, there was no way to remove the heat. The induction heater was not used to reduce the amount of heat accumulating within the vacuum chamber. When the induction heater was utilized, not only was more power consumed but the chocolate would have a lower viscosity than necessary and begin to extrude from the syringe without user input. Fig. 4b and. Fig. 4d displays the discontinuity in the print at the starting position because of the motors being unresponsive when reaching the end of the code.

As shown from the viscosity studies, vacuum-cycled chocolate had a higher viscosity at the operating shear rate. However, to be printable within the vacuum chamber, the reduced pressure also decreased the melting temperature allowing the chocolate to still bond during the vacuum chamber printing. It should be noted the testing and printing environments are different. The printing was done with the pressure constantly decreasing as the print was ongoing. The viscosity test vacuum-cycled the chocolate beforehand and then tested it under constant temperature. The results from the viscosity display standard chocolate is more viscous at the same temperature.

4.2. Stability of 3D bioprinter during launch conditions

4.2.1. Random vibration testing

The results of the random vibration test showed that the printer encountered no visual failure or malfunction after vibrating in all three axes of movement. The x- and y-axis tests shook the printer and produced no real points of failure or malfunctioning. The amount of vibration identified in the x-axis and y-axis tests was much higher than in the z-axis. The z-axis test produced the least amount of vibration and was determined to be negligible in the analysis. Displacement data were also recorded for the x-axis and the y-axis.

Table 6 and Table 7 display the recorded data from each test with the initial height being recorded as well. Notably, corner 2 in the x-axis and y-axis tests was decreasing in height. The difference in displacement between different axes may be due to the asymmetric design of the extruder. This causes the vibration distribution to be different across different corners of the top plate. It could also be attributed to the top plate adjusting to attain an equal height between all corners. The results of the displacement test were consistent across the xaxis and y-axis except corner 2 displayed a negative displacement as shown in Fig. 7 and Fig. 8 respectively. The displacement of the corners is close in value making them consistent across the x and y axes. Corner 3 and Corner 4 were elevated to level the printer. The amount of error for pole 2 is also higher than the other poles, which accounts for the varied displacement in that corner.

Table 6. Recorded corner displacements after vibration testing in the X-axis.

	Corner 1	Corner 2	Corner 3	Corner 4	Average Corner
Initial (±1mm)	194.780	194.880	195.830	195.580	195.268
Test 1 (mm)	0.260	-0.330	0.180	0.330	0.110
Test 2 (mm)	0.200	-0.210	0.090	0.240	0.080
Test 3	0.240	-0.190	0.130	0.290	0.118

Table 7. Recorded corner displacements after vibration testing in the Y-axis

	Corner 1	Corner 2	Corner 3	Corner 4	Average Corner
Initial (±1mm)	194.780	194.880	195.830	195.580	195.268
Test 1 (mm)	0.270	-0.170	0.070	0.410	0.145
Test 2 (mm)	0.230	-0.080	0.040	0.370	0.140
Test 3 (mm)	0.250	0.060	0.140	0.380	0.208

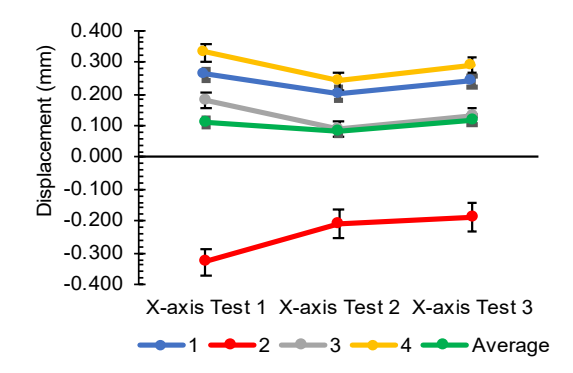


Fig. 7. Displacement of the top plate by each corner during vibration testing of the x-axis

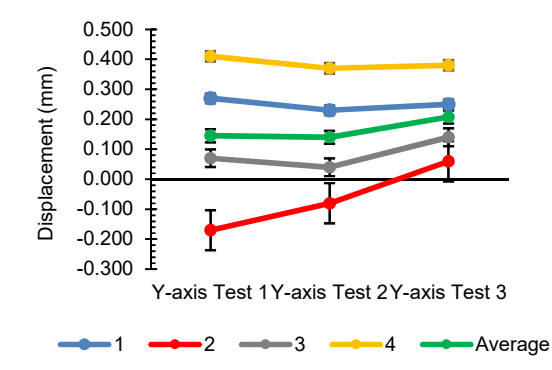


Fig. 8. Displacement of the top plate by each corner during vibration testing of the y-axis

4.2.2. Hammer impact testing

The resonant frequency is the frequency when the oscillation of an object is at maximum amplitude. The peak of the transfer function graphs is where the resonant frequency occurs. Coherence verifies the natural frequency of the printer by determining the linearity of the system. A coherence value of 1 indicates that the natural frequency from the transfer function graph is linear. This means the natural frequency is not time-dependent and capable of being controlled. A coherence value of zero indicates that the system may be non-linear, time-dependent, or both, which corresponds to a low quality of control.

The test was done in three axes: x, y, and z, and was tapped five times to get an average of the readings. The graphs have a frequency range of 0 to 100 Hz. As seen from the random vibration testing, the x and y-directions receive more feedback on the vibrations whereas the z-direction doesn't show a peak within 100 Hz. Fig. 9 depicts the transfer function recorded from the x, y, and z directions of the hammer test respectively. In Fig. 10, the coherence graph is displayed obtained for x, y, and z directions. Accelerometer 1 which was placed on the top of the printer was used for the graphs due to it being closer to the striking point. The other two accelerometers are farther away from the striking point and record less vibration. Using the coherence graph and analyzing accelerometer 1, the linearity of the line depicts that the vibrations are not time-dependent.

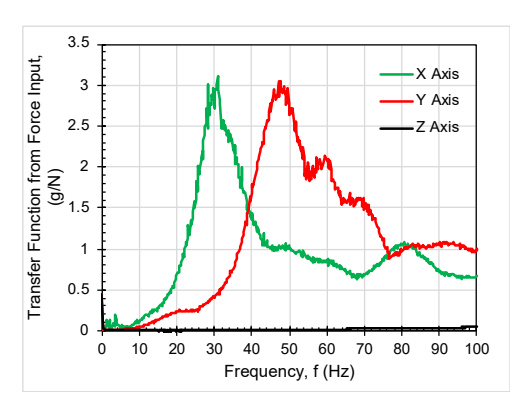


Fig. 9. Transfer function from force input based on the frequency in the x-axis, y-axis, and z-axis from accelerometer 1

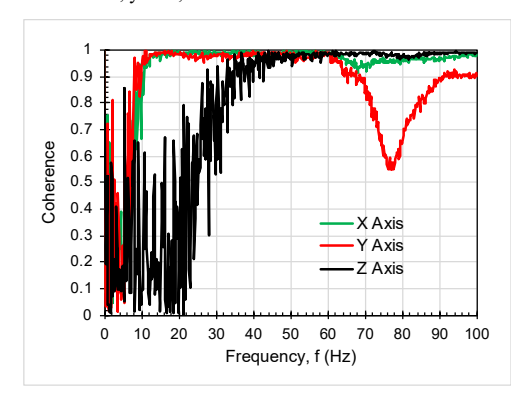


Fig. 10. Resulting coherence based on frequency in the x-axis, y-axis, and z-axis

The recorded resonant frequency displayed in Table 8 is verified by the coherence graphs. Accelerometers 2 and 3 are used to record the residual vibrations that occur when the printer is struck by the hammer during testing. The coherence graph in the z direction displays the coherency, but the resonant frequency is inconclusive in the transfer function graph. This is consistent with the low displacement from the vibration testing, where the frequency for the accelerometer to react in the z direction would have to be higher.

Table 8. Recorded resonant frequency from the hammer test using accelerometer 1

	X Direction	Y Direction	Z Direction
Resonant Frequency (Hz)	~30	~47	Inconclusive

During vibration testing, the asymmetric arrangement of printer components caused the vibration to be displaced differently during the tests resulting in different values for the resonant frequency along different directions. The qualitative data was to visually assess any areas of weakness or any damage or malfunctions occurring at the end of the tests. The addition of the truss elements and increasing the diameter of the structural rods helped to dampen the amount of vibration occurring in the entire system which was one of the improvements during design iterations. The results displayed no visual damage had occurred and the top plate of the printer did not displace more than one millimeter, which was the metric for determining the success of vibration testing. Quantitatively, the displacement of the corners of each structural rod did displace enough to warrant failure. The

physical space constraint of the CubeSat system would have a low margin of extra space, and when accounting for other components (such as power modules, cables, and auxiliary equipment) within the CubeSat, a large displacement could cause damage to these parts or cause the print not to be correctly aligned. A large displacement would have been anything larger than 1 millimeter on any of the corners. Future iterations of the design will use sensors to allow correction in the extruder syringe height if there is a large displacement. The corners where the measurements were recorded would be welded into place to stop any displacement from occurring on the frame.

The results of the hammer impact testing displayed how the printer vibration survivability could be improved. The natural frequency is approximately 30 to 50 Hz in the x-direction and y-direction. These values are essential benchmarks because they indicate that improperly secured parts in the x- and ydirections could potentially fail in higher-vibration environments. However, since the printer was not damaged during or malfunctioned after the random vibration testing at minimum component vibration recommendations, the frequencies are acceptable for this testing. The printer would have to endure a higher dB/oct amount for actual payload testing to pass NASA standards. To improve the resonant frequencies, replacing the material from PLA plastic with anodized aluminum would help due to the higher strength-toweight ratio. The change to anodized aluminum would make the printer rated for extravehicular space travel as well.

5. Conclusion

With space exploration becoming more commercial with continuous rocket testing and space travel, an on-demand AM platform is necessary to allow for flexibility and customizability in manufacturing various products as required. The printer using CubeSat boundary conditions for size, weight, and power consumption, provided a case study to test a low-spatial footprint manufacturing module platform for demonstrating soft material printing. This research focused on the design of an AM platform module that can be placed within a CubeSat system. The constraints of the CubeSat coupled with space boundary conditions create a unique challenge where the power consumption, limited physical space, vacuum pressure environment, structural strength, and remote operation make the design challenging. The main takeaways from this research are (1) the comparison of ambient Earth environment printing vacuum pressure environment displaying how methodology affects printing, how heat distribution of the motors and syringe would have to be managed, and the aesthetics of vacuum printing an organic material; (2) the structural design of a macroscale AM platform to withstand the vibrations of launch conditions.

The data presented showed the potential merit of this concept and the scope for further improvements. The drawbacks of this design are the restricted amount and diversity of printing material, limited printing accuracy, relative simplicity of the printable designs, and structural integrity of printed material. Future generations of the printer will address (1) the printing material volume by redistribution of geometry; (2) diversity of materials by using various heating elements of higher degree; (3) a more sophisticated microcontroller capable

of more precise movement of the motors for more complex designs and improved accuracy; (4) the change from plastic as the structure of the printer to a more space-rated material such as aluminum which can also assist in vibration dampening and structural strengthening; (5) determining shielding for radiation and temperature extremes to protect the electrical systems with the CubeSat. Additionally, the future studies would target systematic design of experiments to study the additive manufacturing process in depth to understand the science and engineering of soft material printing under microgravity as a function of material and process variables.

Through the modular manufacturing methodology, the successful design of mesoscale biomanufacturing AM module platforms would allow for 1) scalability by launching multiple modules), 2) customization through designing various modules to deliver different functions (e.g. different types of materials), and 3) resilience by the virtue of the distribution of various modules and interoperability in case of disturbances or failures. All three merits form the crucial pillar of sustainability of ISM efforts and thus highlight the importance of this research.

Acknowledgments

The authors thank Dr. James Gibert and Dr. Hongcheng Tao for their assistance during the vibration and vacuum testing. They offered to use the shaker for simulating launch conditions and the vacuum chamber during vacuum printing testing.

The authors would also like to thank the Purdue Space Program (PSP) Satellites Team for bringing us the boundary conditions of the CubeSat and design experiment.

References

- [1] Benaroya, H., 2017, "Lunar Habitats: A Brief Overview of Issues and Concepts," REACH, 7–8, pp. 14–33.
- [2] Zocca, A., Wilbig, J., Waske, A., Günster, J., Widjaja, M. P., Neumann, C., Clozel, M., Meyer, A., Ding, J., Zhou, Z., and Tian, X., 2022, "Challenges in the Technology Development for Additive Manufacturing in Space," Chinese J. Mech. Eng. Addit. Manuf. Front., 1(1), p. 100018.
- [3] Trujillo, A. E., Moraguez, M. T., Wald, S. I., Owens, A. C., and de Weck, O. L., 2017, "Feasibility Analysis of Commercial In-Space Manufacturing Applications," AIAA Sp. Astronaut. Forum Expo. Sp. 2017, 409(203999), pp. 1–17.
- [4] Hoffmann, M., and Elwany, A., 2023, "In-Space Additive Manufacturing: A Review," J. Manuf. Sci. Eng., 145(2).
- [5] Thirsk, R., Kuipers, A., Mukai, C., and Williams, D., 2009, "The Space-Flight Environment: The International Space Station and Beyond," Can. Med. Assoc. J., 180(12), pp. 1216–1220.
- [6] Newman, D. J., 2000, "Life in Extreme Environments: How Will Humans Perform on Mars?," Gravit. Space Biol. Bull., **13**(2), pp. 35–47.
- [7] Malshe, H., Bapat, S., Vickers, J., and Malshe, A., 2023, "Factories-in-Space for Servicing, Assembly, & Manufacturing," Manuf. Lett., 38, pp. 24–28.

- [8] Poghosyan, A., and Golkar, A., 2017, "CubeSat Evolution: Analyzing CubeSat Capabilities for Conducting Science Missions," Prog. Aerosp. Sci., 88, pp. 59–83.
- [9] Xu, W., Jambhulkar, S., Zhu, Y., Ravichandran, D., Kakarla, M., Vernon, B., Lott, D. G., Cornella, J. L., Shefi, O., Miquelard-Garnier, G., Yang, Y., and Song, K., 2021, "3D Printing for Polymer/Particle-Based Processing: A Review," Compos. Part B Eng., 223(June), p. 109102.
- [10] Ngo, T. D., Kashani, A., Imbalzano, G., Nguyen, K. T. Q., and Hui, D., 2018, "Additive Manufacturing (3D Printing): A Review of Materials, Methods, Applications and Challenges," Compos. Part B Eng., 143(December 2017), pp. 172–196.
- [11] Nickels, L., 2018, "Office-Based AM Now Open for Business," Met. Powder Rep., **73**(4), pp. 195–197.
- [12] Gonzalez-Gutierrez, J., Godec, D., Kukla, C., Schlauf, T., Burkhardt, C., Holzer Gonzalez-Gutierrez, C. J., Leoben, M., Glöckel-Straße, O., Ass Godec, L. D., Kukla, mont C., Schlauf, I. T., Burkhardt, P. C., and Holzer, P. C., 2017, "Shaping, Debinding and Sintering of Steel Components via Fused Filament Fabrication," 16 th Int. Sci. Conf. Prod. Eng., (June), pp. 8–10.
- [13] Campbell Ian, W. T., 2017, "Markforged: Taking a Different Approach to Metal AM," Met. AM, **3**(2), pp. 113–116.
- [14] Hussain, S., Malakar, S., and Arora, V. K., 2022, "Extrusion-Based 3D Food Printing: Technological Approaches, Material Characteristics, Printing Stability, and Post-Processing," Food Eng. Rev., 14(1), pp. 100– 119.
- [15] Zhang, J. Y., Pandya, J. K., McClements, D. J., Lu, J., and Kinchla, A. J., 2022, "Advancements in 3D Food Printing: A Comprehensive Overview of Properties and Opportunities," Crit. Rev. Food Sci. Nutr., 62(17), pp. 4752–4768.
- [16] Derossi, A., Caporizzi, R., Azzollini, D., and Severini, C., 2018, "Application of 3D Printing for Customized Food. A Case on the Development of a Fruit-Based Snack for Children," J. Food Eng., 220, pp. 65–75.
- [17] Wegrzyn, T. F., Golding, M., and Archer, R. H., 2012, "Food Layered Manufacture: A New Process for Constructing Solid Foods," Trends Food Sci. Technol., 27(2), pp. 66–72.
- [18] Lin, C., 2015, "3D Food Printing: A Taste of the Future," J. Food Sci. Educ., **14**(3), pp. 86–87.
- [19] Terfansky, M. L., and Thangavelu, M., 2013, "3D Printing of Food for Space Missions," (February).
- [20] Jiang, J., Zhang, M., Bhandari, B., and Cao, P., 2020, "Current Processing and Packing Technology for Space Foods: A Review," Crit. Rev. Food Sci. Nutr., 60(21), pp. 3573–3588.
- [21] Kuo, C.-C., Qin, H., Cheng, Y., Jiang, X., and Shi, X., 2021, "An Integrated Manufacturing Strategy to Fabricate Delivery System Using Gelatin/Alginate Hybrid Hydrogels: 3D Printing and Freeze-Drying," Food Hydrocoll., 111, p. 106262.
- [22] McHugh, T., and Bilbao-Sainz, C., 2017, "3D Food

- Printing: A New Dimension in Food Production Processes," Food Technol., **71**(4), pp. 123–125.
- [23] Oluwafemi, F. A., De La Torre, A., Afolayan, E. M., Olalekan-Ajayi, B. M., Dhital, B., Mora-Almanza, J. G., Rivolta, A., and Neduncheran, A., 2018, "Space Food and Nutrition in a Long Term Manned Mission," Proc. Int. Astronaut. Congr. IAC, 2018-Octob(1), pp. 1–21.
- [24] Office of the NASA Chief Engineer, 2017, "Payload Vibroacoustic Test Criteria," NASA Tech. Stand. Syst.
- [25] Voon, S. L., An, J., Wong, G., Zhang, Y., and Chua, C. K., 2019, "3D Food Printing: A Categorised Review of Inks and Their Development," Virtual Phys. Prototyp., 14(3), pp. 203–218.
- [26] VA, A., Udayarajan, C. T., Goksen, G., Brennan, C. S., and P, N., 2023, "A Brief Review on 3D Printing of Chocolate," Int. J. Food Sci. Technol., **58**(6), pp. 2811–2828.